Preprint Cambridge Centre for Computational Chemical Engineering ISSN 1473 – 4273

A high-dimensional, stochastic model for twin-screw granulation
Part 1: Model description

Andrew D. McGuire [1], Sebastian Mosbach [1], Kok Foong Lee [1],
Gavin Reynolds [2], Markus Kraft [1,3]

released: 17 October 2017

[1] Department of Chemical Engineering
and Biotechnology
University of Cambridge
New Museums Site
Pembroke Street
Cambridge, CB2 3RA
United Kingdom
E-mail: mk306@cam.ac.uk

[2] Pharmaceutical Technology & Development
AstraZeneca
Charter Way
Macclesfield, SK10 2NA
United Kingdom
E-mail: gavin.reynolds@astrazeneca.com

[3] School of Chemical
and Biomedical Engineering
Nanyang Technological University
62 Nanyang Drive
Singapore 637459
E-mail: mk306@cam.ac.uk

Preprint No. 191

Keywords: granulation, twin-screw, stochastic, population balance

Edited by
Computational Modelling Group
Department of Chemical Engineering and Biotechnology
University of Cambridge
New Museums Site
Pembroke Street
Cambridge CB2 3RA
United Kingdom

Fax: + 44 (0)1223 334796
E-Mail: c4e@cam.ac.uk
World Wide Web: http://como.cheng.cam.ac.uk/

Abstract

In this work we present a novel four-dimensional, stochastic population balance model for twin-screw granulation. The model uses a compartmental framework to reflect changes in mechanistic rates between different screw element geometries. This allows us to capture the evolution of the material along the barrel length. The predictive power of the model is assessed across a range of liquid-solid feed ratios through comparison with experimental particle size distributions. The model results show a qualitative agreement with experimental trends and a number of areas for model improvement are discussed. The stochastic treatment of the model allows the particle description to be readily extended to track more complex particle properties and their transformations.

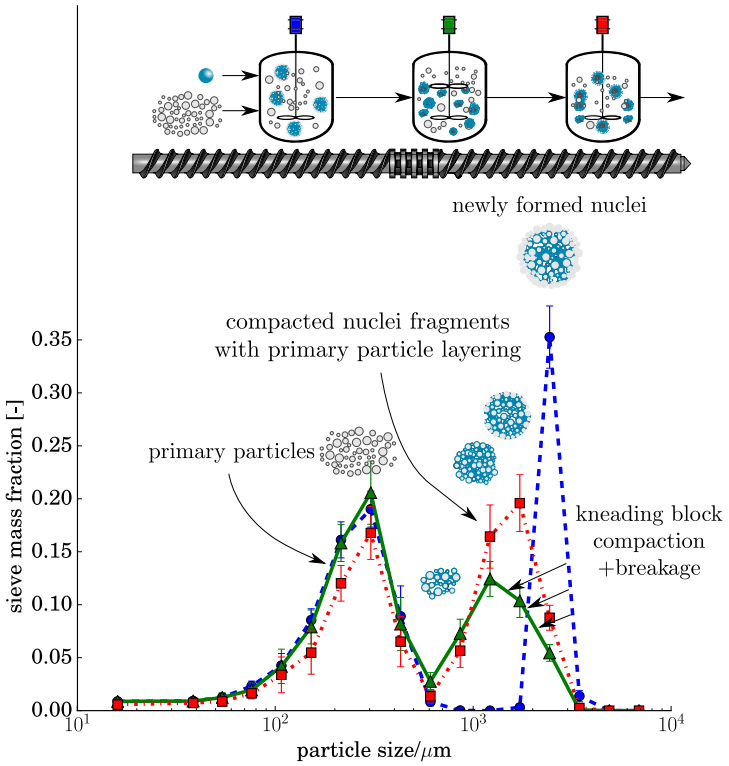

Highlights

- A novel, four-dimensional population balance model for twin-screw granulation is presented
- Particle compositions are resolved along the screw barrel
- The model's performance is assessed at different liquid-solid feed ratios using experimental data
- We observe qualitative agreement with experimental trends
- The model framework can be readily extended to higher dimensions

Contents

1 Introduction

Granulation (also known as agglomeration, pelletisation or balling) is a common method of particle manufacture. The formation of granules is a key process in the food industry, in formation of tablets within the pharmaceutical industry and in the production of fertilisers [29]. The granular product will have an optimum size (typically a distribution), porosity, solubility, mechanical strength, shape and flow-ability amongst other properties dictated by the specific application. Granules have several advantages over a simple mixture of the raw ingredients such as better flow-ability; better transport properties (such as limited separation of components and reduced risk of powder explosions); dissolution behaviour and controlled release of Active Pharmaceutical Ingredients (API) [7, 53].

Twin-screw granulation (TSG) is a relatively new method of continuous granule production and is currently subject to a high degree of research as a viable alternative to batch granulation. TSG consists of a barrel with two co-rotating screws into which raw excipient/API are fed in conjunction with a liquid binder as illustrated in Figure 1. In these systems, the screws and barrel wall impart a shear force on the material, forming granules which are then conveyed along the barrel towards the outlet, undergoing a number of transformations such as growth/attrition along the way, depending on the processing conditions.

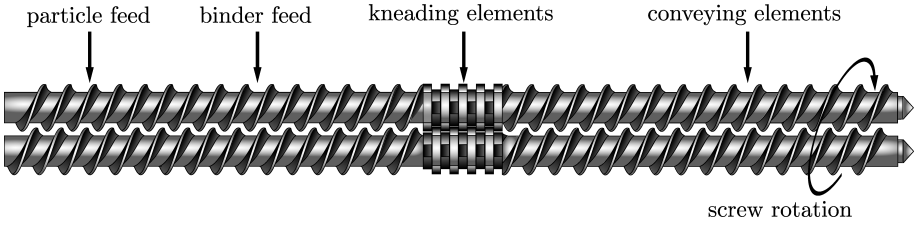

Figure 1: *twin-screw granulator*

TSG systems have shown many advantages over traditional batch production methods such as the ability to: produce flow-able granules with high API content [51]; reduce plant foot print [14]; minimise the use of API/excipient during formulation development and ease the scale-up from development to full production. [57].

Another advantage of TSG equipment is the variable configuration of the device available to the operator during formulation development. Each screw in the TSG system is composed of numerous screw *elements* which may be of varying geometry. Different types of element act differently on the particle mass passing through them and thus the screw element configuration may be altered to produce a granular product with different physical properties. The screw speed, liquid feed rate and powder feed formulation may also be varied in this way, resulting in a system with an exceptionally large operating space. The complexity and variability of the TSG system therefore requires a deep understanding of the underlying process in order to predict, and more importantly, control the properties of the resulting granules, in line with the philosophy of Quality by Design [24].

Experimental studies have probed the effects of screw element configuration on the physical properties of the granular product from TSG systems and tried to identify the role of

specific types of screw element [22, 38, 48, 56]. Dhenge *et. al.* have investigated the effect of powder feed rate [17] and binder viscosity [19] while Li et al. [37] and Vanhoorne et al. [54] have assessed the impact of the physical properties of the API on the TSG process. Hagrasy et al. [26] investigated the effect of powder feed formulation and liquid-solid mass feed ratio on product size/porosity distribution and Saleh *et al.* [47] investigated the effect of binder delivery method on the TSG system. Though the number of experimental investigations is extensive, the large operating window of TSG systems often limits the applicability of these results to local regions of the operating space. The comprehensive review of the experimental TSG literature by Seem et al. [49] shows a complex interplay between the role of each screw element type, the overall screw configuration, feed formulation and liquid flowrates on the observed experimental trends. This emphasises the need for a particle-scale model of TSG that can accurately predict the physical properties of the bulk granular product. Ultimately, the inversion of such a model could then be carried out and coupled with process control systems to allow specification and control of product specification in TSG systems.

Granular systems are generally modelled using population balance models (PBM) [5, 7–12, 15, 30, 46]. TSG specific PBMs have been developed, ranging from one [34] to three dimensional particle models [3, 4]. A lumped parameter method is typically used to estimate additional particle properties beyond those explicitly tracked by the model [3]. Flow information and collision data have been incorporated into TSG models through couplings with alternative modelling frameworks such as the discrete element method (DEM) [3] and experimental near-infrared chemical tracing [32, 34]. Many of these TSG PBM studies have shown results in qualitative agreement with the experimental studies; however, quantitative predictions have proven to be much more challenging. One reason for this could be over-simplification of the system within the models. All of the existing TSG PBM models are numerically solved using variations of the sectional method [28]. Such a numerical approach ultimately limits the model dimensionality as high dimensional models become computationally unfeasible, thereby placing a limit on model complexity.

In the first part of this two-part study we present a four-dimensional stochastic population balance model of a TSG system. This TSG model extends the batch granulation model introduced by Braumann et al. [8] and further developed by Lee et al. [35], to a continuous compartmental framework. By stochastically evolving the particle ensemble in time, the particle representation may be arbitrarily complex. The additional particle dimensions not afforded to traditional sectional methods can then be integrated in the twin-screw process description. In the second part of this study we present and analyse the numerical methods developed to overcome the numerical challenges inherent to stochastic modelling of twin-screw systems and solve the TSG model described in this paper. The model is used to simulate the experiments carried out by Hagrasy et al. [26], specifically those testing the effect of varying liquid-solid ratio (LSR) using a *Lactose Impalpable* placebo feed formulation.

The remainder of the paper is structured as follows: firstly we present an overview of the existing population balance model for high shear granulation developed by Braumann et al. [8] and Lee et al. [35]. A detailed account of the twin-screw model mechanisms is given in Section 2.2. The parameter estimation methodology used to evaluate unknown process rate constants is then briefly discussed, followed by a presentation and discussion

of the main results in Section 4. Finally, the main findings and future recommendations for TSG modelling are summarised in Section 5.

2 Methodology

2.1 Population balance model

A four-dimensional population balance model is used as the base for the twin-screw granulation model in this study. A general account of the underlying population balance model and the twin-screw specific features are outlined in this section. For a detailed description of the underlying population balance model, the reader is directed to [10, 35].

Building on the work of Lee et al. [35], the granulator is represented by a series of connected, well-mixed *compartments* filled with particles. In this work we use the type-space $x = (s_o, l_e, l_i, p)$ to describe each particle, where: s_o is the original solid volume , l_e is the external liquid volume , l_i is the internal liquid volume and the pore volume as illustrated in Figure 2. Internal liquid only exists within the pore volume and the remaining pore volume is occupied with gas. The same particle vector is capable of representing any of

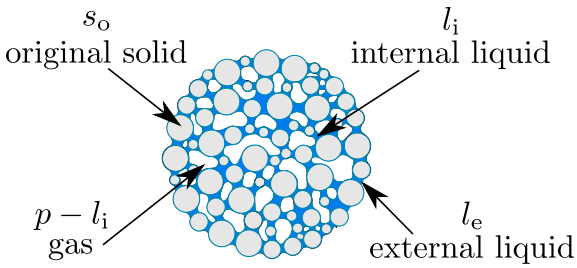

Figure 2: *Particle description.*

the phases present in a placebo granulation system, namely: primary particles, granules and free liquid droplets.

Using this particle description, the total particle volume is:

$$v(x) = s_o(x) + l_e(x) + p(x) \tag{1}$$

and the particle porosity is defined as:

$$\varepsilon(x) = \frac{p(x)}{v(x)}. \tag{2}$$

Particles are assumed to be spherical for the purposes of computing particle surface areas and diameters, however, all non-liquid particles are assumed to have surface asperities with characteristic length scale H_a. These asperities, along with other properties, control the likelihood of successful coalescence between two particles, described further in Section 2.2.

2.2 Twin-screw particle processes

The particles ensemble is evolved in time through a mixture of particle *jump* events and continuous processes as shown in Figure 3. The possible jump events are: nucleation, particle collision (which may or may not lead to rebound, coalescence and particle compaction), particle breakage and particle transport (between compartments). Liquid penetration (transforming external liquid to internal liquid) is carried out as a continuous particle process.

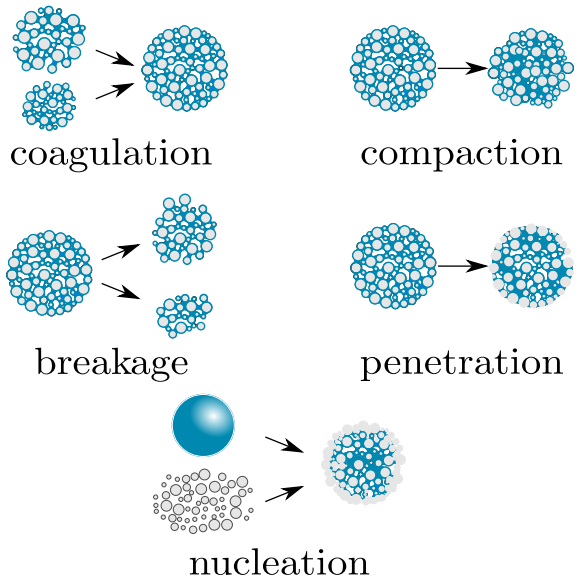

Figure 3: *Particle processes permitted in the TSG model.*

Liquid addition/nucleation

In TSG, primary agglomerates are generally formed by way of immersion nucleation [18, 19, 50] as small primary particles diffuse into large liquid droplets that are incident on the surface of the powder bed. This mechanism is relevant for TSG, as liquid will typically be added without the use of an atomisation nozzle, and primary particles are typically of the order of 10 to 100μm. It is hypothesised that these liquid-rich primary agglomerates (or *nuclei*) are subject to compaction and breakage, particularly in kneading elements, as described by the destructive nucleation mechanism of Vonk et al. [58]. Here we adapt an interpretation of the immersion nucleation mechanism to the type-space of the current model.

The nucleation process begins with the inception of a large droplet. These droplets are mono-disperse and incepted into the liquid inception zone. The droplet volume defines the initial state of the nuclei particle x_{nuc} before it has interacted with the particle bed, hence,

$$x_{\text{nuc}}^{\text{start}} = (0, 0, v_{\text{drop}}, 0). \tag{3}$$

As in Lee et al. [35] the rate of droplet inception is given by:

$$R_{\text{incept,droplet}}(z) = \frac{\dot{V}_l}{V_{\text{real}}(z) v_{\text{drop}}}, \tag{4}$$

where $V_{\text{real}}(z)$ is the volume of the compartment z, $\dot{V}_l$ is the liquid flow-rate delivered to system and v_{drop} is the volume of the droplets being incepted. $\dot{V}_l$ is given by LSR and the liquid density ρ_{l} as:

$$\dot{V}_l = \frac{(\text{LSR})\dot{M}_{\text{feed}}}{\rho_{\text{l}}}. \tag{5}$$

In the model, the incepted droplet results in the formation of a single nucleus, as no rewetting is considered due to the assumption of no back mixing in the liquid addition compartment, hence:

$$R_{\text{nuc}}(z) = R_{\text{incept,droplet}}(z). \tag{6}$$

The probability that a particle will be selected to form part of a nucleus is assumed to be proportional to the volume of the particle. Additionally, it is postulated that there is a maximum particle size that can be integrated into the nucleus. In this study we set the size limit for integration $v_{\text{nuc}}^{\max} = v_{\text{drop}}$. It is presumed that the addition of particles to the droplet (to form a nucleus) happens instantaneously as the droplet enters the compartment. These model properties can be expressed using a nucleation kernel of the form

$$K_{\text{nuc}}(z,x,y,t) = \begin{cases} R_{\text{nuc}}(z)\min(v(x),v(y))/\sum_{j=1}^{N(z,t)} v(x_j) & \text{if } \min(v(x),v(y)) < v_{\text{drop}}, \\ 0 & \text{otherwise,} \end{cases} \tag{7}$$

where x and y are the particles involved in each particle addition to the nucleus (either x or y being the nucleus). This form of kernel is suitable when the volume of nucleus is always greater than the particle to be added to it (as is the case in this study) i.e. such that the term $\min(v(x),v(y))$ is always the volume of the particle to be added.

As a particle is added to the partially formed nucleus, this results in the drying of the nucleus surface (internalisation of liquid). The degree of drying is assumed to be dependent on the state of the particle being added. The change in the nucleus particle properties induced by the addition of particle x_i to the nucleus is given by

$$s_{\text{o}}(x_{\text{nuc}}) \leftarrow s_{\text{o}}(x_{\text{nuc}}) + s_{\text{o}}(x_i) \tag{8}$$

$$\begin{aligned} l_{\text{e}}(x_{\text{nuc}}) \leftarrow & l_{\text{e}}(x_{\text{nuc}}) \\ & - \min([\phi_{\max} - \phi(x_i)]\mathbb{1}\{\forall\phi(x_i) \le \phi_{\max}\}s_{\text{o}}(x_i), l_{\text{e}}(x_{\text{nuc}})), \end{aligned} \tag{9}$$

$$\begin{aligned} l_{\text{i}}(x_{\text{nuc}}) \leftarrow & l_{\text{i}}(x_{\text{nuc}}) + l_{\text{i}}(x_i) + l_{\text{e}}(x_i) \\ & + \min([\phi_{\max} - \phi(x_i)]\mathbb{1}\{\forall\phi(x_i) \le \phi_{\max}\}s_{\text{o}}(x_i), l_{\text{e}}(x_{\text{nuc}})), \end{aligned} \tag{10}$$

$$p(x_{\text{nuc}}) = l_{\text{i}}(x_i)/s^*. \tag{11}$$

Here $\phi(x_i)$ is the liquid saturation level of the particle to be added, given as:

$$\phi(x) = \frac{l_{\text{i}}(x) + l_{\text{e}}(x)}{s_{\text{o}}(x)}, \tag{12}$$

and $\phi_{\max}$ is the maximum level of liquid saturation in the nuclei. To quantify this value we follow a similar approach to that taken by Barrasso and Ramachandran [2] to model the size of newly formed nuclei. This approach is consistent with the nucleation mechanism described by Iveson et al. [29], where nuclei are formed by way of droplet penetration into a porous bed. This is captured by the relation:

$$\phi_{\max} = \frac{(1-\varepsilon_{\text{bed}})s^*}{\varepsilon_{\text{bed}}}, \tag{13}$$

where ε_{bed} is the bed packing fraction and s^* is the maximum internal pore liquid saturation level of the nuclei.

The addition of particles to the nucleus in the nucleation processes ceases when $l_{\text{e}}(x_{\text{nuc}}) = 0$. It is noted that the particle transform in (9) allows the addition of over-saturated particles to the nucleus to generate more surface nuclei liquid and hence allow for further particle addition to or growth of the nucleus.

Collision/compaction

Model particles may undergo binary collisions. The rate of collision between particles x_i and x_j is modelled using the size independent collision kernel:

$$K_{\text{col}}(z, x_i, x_j) = n_{\text{screw}} k_{\text{col}}(z), \tag{14}$$

where n_{screw} is the screw speed and k_{col} is the collision rate constant. Each particle collision leads to the compaction of the particles involved. This is modelled as a porosity reduction described by:

$$\Delta\varepsilon(x) = \begin{cases} k_{\text{comp}}(z)[\varepsilon(x) - \varepsilon_{\min}], & \text{if } \varepsilon(x) \geq \varepsilon_{\min}, \\ 0, & \text{otherwise}, \end{cases} \tag{15}$$

where k_{comp} is the compaction rate constant and $\varepsilon_{\min}$ is the minimum porosity permitted.

Several experimental studies [19, 22, 49, 55, 56] have concluded that internal liquid is squeezed to the surface of nuclei/nuclei fragments in areas of high compaction such as kneading blocks. This newly surfaced liquid then permits the layering of dry primary material onto the surface of the compacted particles. To described the movement of liquid during this squeezing process, some of the internal liquid is moved to external liquid. The amount of liquid transferred $l_{i\to e}$ is proportional to the relative change in pore volume as described by the following relation:

$$l_{i\to e} = \Delta p_{\text{comp}} \left(\frac{l_{i,o}}{p_o} \right), \tag{16}$$

where $l_{i,o}$ and p_o are the internal liquid and pore volumes, respectively, prior to compaction and Δp_{comp} is the change in pore volume associated with a compaction event. Consistency between (1), (2) and (16) requires:

$$\Delta p_{\text{comp}} = p_o - \frac{\varepsilon_1 (s_{\text{o}} + l_{e,o} + l_{i,o})}{1 - \varepsilon_1 \left(1 - \frac{l_{i,o}}{p_o}\right)}. \tag{17}$$

Here, $l_{e,o}$ is the external liquid volume prior to compaction and ε_1 is the post compaction porosity.

Whether or not a particular collision is successful (resulting in coagulation of the parent particles) is governed by the Stokes criterion [23]. This is detailed in the context of the particle model in [10, 35]. Following the approach of Goodson *et al.* [25], if a coagulation event is successful then a fraction of the external liquid l_e from the particles involved in the collision becomes internal liquid l_i in the newly formed particle. The pore volume of the newly formed particle is further modified for successful collisions. This change is dependent on the surface area of the particles involved and the coefficient of restitution e_{coag} as described in [10]. The resulting particle process may be described as:

$$\begin{aligned} \text{Coalescence successful: } & (x_i),(x_j) \rightarrow (T_{comp}(x_i+x_j)), \\ \text{Coalescence unsuccessful: } & (x_i),(x_j) \rightarrow (T_{comp}(x_i)),(T_{comp}(x_j)), \end{aligned}$$

where T_{comp} is the compaction transformation.

Breakage

As in Braumann et al. [10], particles may undergo binary breakage and the daughter distribution is described by a beta distribution. The skewness of this beta function is determined by parameters $\alpha_{daughter}$ and $\beta_{daughter}$. The breakage transform is:

$$T_{break}(x_i) \rightarrow (x_j),(x_i - x_j), \tag{18}$$

where T_{break} is the breakage operator.

The choice of breakage kernel varies significantly across the literature, reflecting the relatively poor understanding of this particle process. Breakage kernels generally take the form of a power law, applied to the particle volume, which may have a fitted [4] or predefined exponent [34] and may also be partially dependent on the particle pore volume [10]. In preliminary model development, various power law kernels were tested and assessed through the PSD evolution of particles along the network. A volume based-kernel with direct proportionality was settled upon, due to its simplicity and the fact that it resulted in sensible PSD evolutions along the network. In the future, more complex breakage kernels could be investigated, with dependencies on particle properties such as the degree of compaction, internal liquid etc. and on screw geometry. Primary particles and particles with volume less than v_{parent}^{min} are considered to be unbreakable. The breakage frequency function for particle x is:

$$g_{break}(z,x) = \begin{cases} k_{att}(z) n_{screw}^2(z) v(x), & \text{if } v(x) \geq v_{parent}^{min} \text{ and } l_e(x) + l_i(x) + p(x) \neq 0, \\ 0 & \text{otherwise,} \end{cases} \tag{19}$$

where k_{att} is the attrition rate constant.

It follows that the total breakage rate R_{break} in compartment z is given by:

$$R_{break}(z,t) = \sum_{i=1}^{N(z,t)} g_{break}(z,x_i). \tag{20}$$

Penetration

As previously mentioned, binder penetration is modelled as a continuous processes within

the model. The penetration process is intended to capture the flow of binder from the particle surface to the interior of the particle, driven by capillary forces. As in Braumann et al. [11] this involves the transformation of l_e to l_i at rate r_{pen}, controlled by the rate constant k_{pen} as:

$$r_{pen}(z,x) = k_{pen}(z)\mu_{binder}^{-1/2} l_e(x)(p(x) - l_i(x)), \tag{21}$$

where μ_{binder} is the viscosity of the binder.

Each particle in the ensemble is modified between stochastic jump events according to the following set of ordinary differential equations:

$$\frac{ds_o}{dt} = 0, \quad \frac{dl_e}{dt} = -r_{pen}, \quad \frac{dl_i}{dt} = r_{pen}, \quad \frac{dp}{dt} = -r_{pen}.$$

2.3 Compartmentalisation of the twin-screw

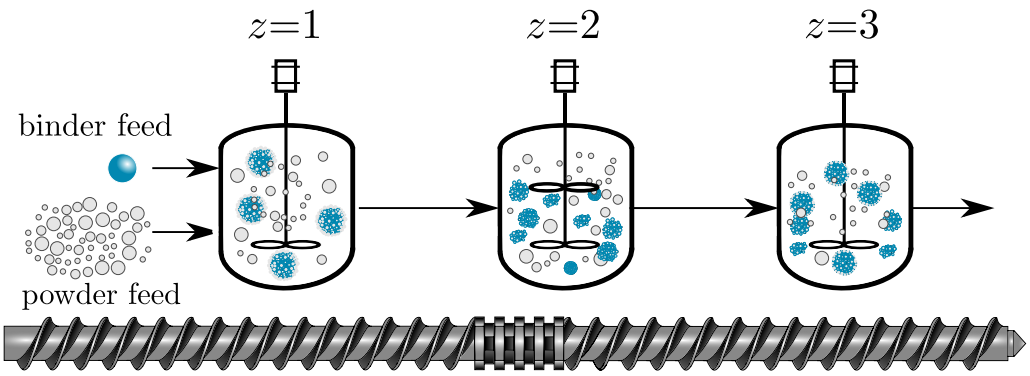

Figure 4: *Compartmental representation of the twin-screw.*

The experimental studies by Hagrasy et al. [26] were used to test the model. This study employed a screw configuration consisting of a conveying section followed by a section of conveying/kneading elements and then an additional conveying section. This is modelled as a series of three well-mixed compartments as illustrated in Figure 4. Compartments $z = 1$ and $z = 3$ are assumed to represent pure conveying sections, which are assumed to share the same set of rate constants. Droplet inception/nucleation is only permitted in the first compartment. The central conveying/kneading compartment ($z = 2$) is permitted to have different collision, breakage and compaction rates, relative to the pure conveying zones. The penetration rate is assumed to be a material constant and thus is the same in each compartment.

It is assumed that transformation of the feed material is limited prior to the point of liquid injection of the twin-screw system. For this reason the twin-screw system in modelled from the liquid injection point onwards.

Particle transport

The rate of particle outflow from compartment $z \in \{1,2,3\}$ is given by:

$$R_{\text{outflow}}(z) = \frac{N(z,t)}{\tau(z)}, \tag{22}$$

where $N(z,t)$ and $\tau(z)$ are the number of particles and characteristic residence time of compartment z at time t, respectively. The rate of inflow into compartment $z+1$ from compartment z is then given by:

$$R_{\text{inflow}}(z+1,t) = \frac{V_{\text{samp}}(z+1,t)}{V_{\text{samp}}(z,t)} R_{\text{outflow}}(z,t). \tag{23}$$

As in the work of Barrasso et al. [4] (which used the same experimental test case as that used in this study) the residence times are assumed to be equal in all compartments with $\tau = 2.67$s. In future work this assumption could be relaxed by incorporating information from experimental twin-screw residence time studies [32, 33] and PEPT investigations [50].

Particle Inception/Initialisation

Similar to liquid inception, the rate of inception of primary particles into each compartment is given by:

$$R_{\text{incept}}(z) = \begin{cases} \dot{M}_{\text{feed}}/(V_{\text{real}}(z)\bar{m}_{\text{feed}}), & \text{if } z = 1, \\ 0, & \text{otherwise}, \end{cases} \tag{24}$$

where and $\bar{m}_{\text{feed}}$ is the average arithmetic mass of the feed particles. In this study, each compartment is assumed to be of equal volume and thus, $V_{\text{real}}(z) = V_{\text{TSG}}/k_{\text{reac}}$ where n_{reac} is the number of compartments in the network and V_{TSG} is the total volume of the TSG system. The primary particle distribution for inception is derived from the volume fraction distribution $q_3(d)$ presented in [26] for the *Lactose Impalpable* excipient grade. Here, $q_3(d)\mathrm{d}d$ is fraction of the total particle volume contained within the size range d to $d + \mathrm{d}d$. This is converted into a number distribution $q_0(d)$ for use in the model using the relation [1]:

$$q_0(d) = \frac{q_3(d)d^{-3}}{\int_0^\infty q_3(d)d^{-3}\mathrm{d}d}. \tag{25}$$

Each compartment is assumed to be filled with primary particles at $t = 0$.

3 Parameter estimation

The unknown rate constants (seven in total) are estimated using experimental PSDs from Hagrasy et al. [26] at LSR values of 0.15, 0.25 and 0.35. The quality of the model fit against the experimental data is quantitatively measured using a weighted sum-of-squares objective function OF over all N_{exp} experimental conditions and N_{response} model/experimental responses as:

$$OF = \sum_{i=1}^{N_{\text{exp}}} \sum_{j=1}^{N_{\text{response}}} \left(\frac{y_{j,i}^{\text{model}} - y_{j,i}^{\text{exp}}}{\sigma_j} \right)^2. \tag{26}$$

Here, $y_{i,j}^{\text{model}}$ is the j^{th} model response for the i^{th} LSR value used and $y_{j,i}^{\text{exp}}$ is the associated experimental response. Mass based percentiles diameters d25, d50, d75 and d95 of the granular product are used as the model/experimental responses. These are weighted, respectively, using weighting factors σ of 25μm, 50μm, 75μm and 95μm.

The geometry of the objective function is highly complex, containing multiple ridges and local minima. For this reason, we perform a quasi-random search over the parameter space, followed by a (more local) Hooke-Jeeves optimisation [27]. The initial search is carried out by generating a quasi-random sequence of rate constant vectors known as Sobol sequences [6]. Sobol sequences are used in order to spread the model evaluation points more evenly across the parameter space. The Hooke-Jeeves algorithm is selected for the local optimisation since it is a 'derivative-free' optimisation technique. This characteristic is highly desirable in the context of this paper, since derivative approximation by finite differences is problematic with models whose response is subject to stochastic noise. Five Hooke-Jeeves optimisations are carried out, starting from each of the five best Sobol points (i.e. those with the lowest OF value).

Preliminary parameter estimation showed that very similar product PSDs could be obtained for very different sets of rates constants. For example, using the same wide search space for the breakage rate constant k_{att} in both the pure conveying and partial kneading section may result in a situation in which most of the breakage occurred in the conveying sections and very little in the partial kneading section and vice-versa, both giving relatively similar product PSDs. Since only the final PSD is used in the fitting process (mid-barrel experimental PSD data was not available), unphysical PSD evolutions along the network are not penalised by the objective function. Hence, such PSD evolutions must be eliminated through careful selection of the search space for each rate constant, reflecting what is know from experimental investigation. As previously discussed, the body of experimental TSG literature would suggest that the breakage and compaction rates in the kneading element and significantly higher than those present in pure conveying sections (though conveying section are known to break large agglomerates using a cutting action [38]). Thus, the parameter limits for k_{comp} and k_{att} in the central, partial kneading compartment ($z = 2$) are chosen such that they are higher than those of the pure conveying compartments ($z = 1, 3$). To assess the predictive power of the model, the optimised rate constants are then used to model two additional experimental cases with intermediate LSR values of 0.2 and 0.3.

Table 1: *Rate constant bounds used in the parameter estimation process.*

Compartment index z	1,3			2			1-3
Parameter	k_{col}	k_{att}	k_{comp}	k_{col}	k_{att}	k_{comp}	k_{pen}
Unit	m^3	m^{-1}s	-	m^3	m^{-1}s	-	$\text{kg}^{\frac{1}{2}}\text{m}^{-\frac{7}{2}}\text{s}^{-\frac{3}{2}}$
Lower bound	10^{-12}	1.68×10^{4}	0.01	10^{-12}	1.68×10^{6}	0.6	10
Upper bound	10^{-9}	1.68×10^{7}	0.6	10^{-9}	1.68×10^{10}	1.0	10^{6}
Scaling	Log	Log	Linear	Log	Log	Linear	Log

Table 2: *Summary of simulation parameters.*

Parameter	Type	Value	Unit
d_{drop}	Operating parameter	2×10^{-3}	m
$\dot{M}_{\text{feed}}$	Operating parameter	4.0	kg hr^{-1}
n_{screw}	Operating parameter	6.67	rev s^{-1}
$V_{\text{real,T}}$	Equipment geometry	4.05×10^{-5}	m^3
e_{coag}	Material property	0.2	-
ρ_{l}	Material property	998	kg m^{-3}
ρ_{s}	Material property	1545	kg m^{-3}
μ_{binder}	Material property	10^{-3}	Pa s
d_{max}	Model parameter	3.31×10^{-6}	m
d_{min}	Model parameter	8.26×10^{-4}	m
H_{a}	Model parameter	5×10^{-6}	m
k_{reac}	Model parameter	3	-
$v_{\text{parent}}^{\text{min}}$	Model parameter	2.5×10^{-5}	m
$v_{\text{nuc}}^{\text{max}}$	Model parameter	v_{drop}	m^3
V_{compart}	Model parameter	1.35×10^{-5}	m^3
α_{daughter}	Model parameter	5.0	-
β_{daughter}	Model parameter	2.0	-
ε_{min}	Model parameter	0.5	-
τ	Model parameter	2.76	s
ϕ_{max}	Model parameter	1.08	-

The parameter estimation steps are carried out using the Model Development Suite (MoDS) [41]. MoDS is an advanced software package capable of analysing 'black-box' models. MoDS has been successfully used in numerous applications, from the global sensitivity analysis of a silica nanoparticle model [40], to the experimental design and parameter estimation of a combustion engine model [42] and more [13, 39, 43, 45].

4 Results and discussion

In this section we present the simulation results using the optimised rate constants derived from parameter estimation. In Section 4.1 we analyse the model results in the context of the experimental data at LSR values used in the fitting and at a number of intermediate LSR values. This is followed by an analysis of the model PSD evolution along the length of the screw barrel in Section 4.2.

The product ensembles are sieved using a sieve set starting from 32μm to 8064μm using a $\sqrt{2}$ geometric progression. Sieve mass fractions are plotted against the mid-point of the corresponding sieve intervals. Statistical errors estimations for these parameters are reported as 90% confidence intervals.

4.1 The effect of liquid flowrate on particle size distribution

A comparison between the model and experimental product PSD is presented in Figure 5. There is an obvious trend in the results where by the intensity of the primary particle

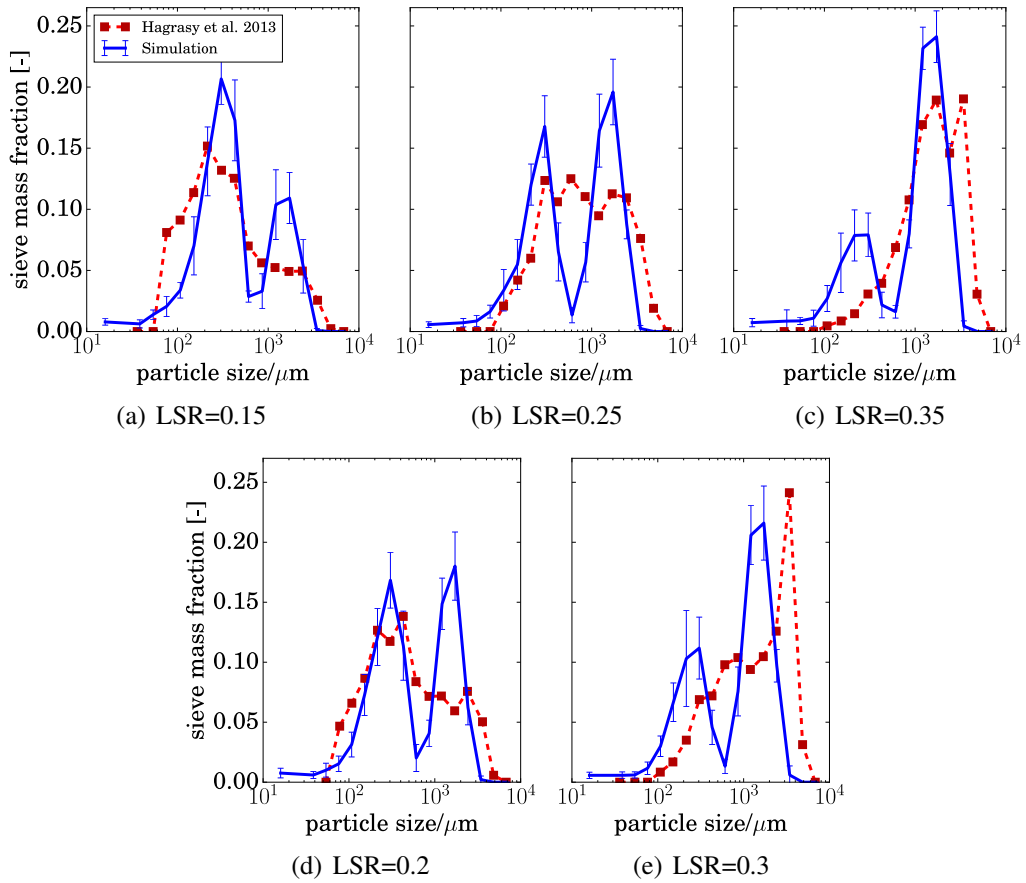

Figure 5: *Simulation PSDs compared with the experimental results of Hagrasy et al. [26]. LSR values which were used in the fitting of the rate constants are presented in (a)-(c) and 'blind tested' intermediate LSR values in (d) and (e).*

mode is reduced with increasing LSR, leading to a reduction in the fines and a larger mean granule size, as observed in TSG experiments [16, 18, 49]. The main disparities occur at higher LSR values where the largest particles size classes produced in the experiment are not captured by the model. The model PSD is bimodal in all cases, consisting of a primary particle mode and an additional mode composed of nuclei fragments which have gone through breakage, coagulation and compaction processes. Such bimodality is generally a feature of TSG product PSD. Hagrasy et al. [26] hypothesised that the inherently bimodal nature of the twin-screw device was a result of the liquid addition method, resulting in a non-uniform liquid distribution. El Hagrasy and Litster [22] also observed that the liquid distribution becomes more uniform with the addition of more kneading blocks. The experimental PSD for low to moderate LSR in Figure 5 may well be evolved from a more pronounced bimodal distribution, with a degree of overlap between the modes.

Such a distribution would be subjected to reduction in intensity along the barrel length. The current model appears to fail in capturing some of the more subtle processes that lead to the mitigation of this bimodality, even in the presence of relative few kneading elements.

There is a clear over-prediction of fines by the model at high LSR values (Figure 5(c) and 5(e)). This may indicate the need for a layering mechanism in the model. This would allow primary particles to become attached to the surface of larger, surface wet agglomerates as a rapid continuous process or additional particle jump process. This would ultimately lead to the separate treatment of the rates/particle transforms associated with agglomerate-primary and agglomerate-agglomerate collisions. Such layering mechanisms have been implemented in the context of a sectional TSG model by Barrasso and Ramachandran [2] and a stochastic model for a high-shear batch mixer by Oullion et al. [44]. The failure to produce the pronounced peak at 4000μm in the case where LSR=0.3 may also indicate that a less aggressive/more versatile breakage kernel (possibly with a variable volume exponent) may be required in the future. This peak may also correspond to particles which have become strengthened through compaction in the kneading elements. Again, such structural changes may need to introduced into the breakage functional to capture the resistance of such particles to further breakage.

Moving to the lower LSR operating range, the disparity between model and experiment in the lowest sieve classes (Figures 5(a) and 5(d)) indicates that, in the real system, large primary particles and/or agglomerates may undergo attrition along the barrel length, therefore acting as a source of 'fines'. Another possible explanation for this discrepancy is that preferential incorporation of larger primary particles in the nucleation mechanism of the model in more pronounced that it is in the real system. Dhenge et al. [19] showed that the material in the barrel became less cohesive with decreasing LSR, resulting in a material that was less resistant to flow and subject to shorter residence times (though this was only tested to LSR values as low as 0.25). This reduction in residence time indicates a lower degree of barrel filling at lower LSR values and may, as suggested by Thompson and Sun [52], result in the material not being protected from the high shear zone at the barrel wall, causing subsequent attrition of largest primary particles in the low LSR regime. Since the breakage of dry primary particles is distinct from the breakage of wet agglomerates, (which may be able to deform and elongate) it is likely that distinct breakage models are required to accurately capture the breakage process for each phase.

Across the complete LSR operating range, the discrepancies between the model and experimental PSD in Figure 5 may have been affected, to some degree, by the varying aspect ratio of particles produced experimentally. It is known that the aspect ratio of particles generally decreases with increasing LSR producing more rounded particles [16, 19, 31], however, as demonstrated by Hagrasy et al. [26], this breaks down at very high LSR. At this high LSR operating range, long extrudate like particle are produced as the mixture becomes more of a paste, making the geometrical variations particularly hard to capture from a modelling perspective. Ultimately, the presence of particles with high aspect ratios may skew the sieve analysis, depending on the particle orientation. It will also affect the nature of subsequent particle breakage and growth. In the current model, particles are considered to be spherical. More complex particle descriptions with element-specific shape transformations may need to be taken into account in future modelling works. Due

to the highly extensible nature of stochastic models, it is possible to track such additional features without significantly affecting the computational cost of the solution process. Nevertheless, work would be required to elucidate the effects of each type of element and how these effects depend on the properties of the particles involved.

Another potential source of error in the model is the assumption of equal residence times across all compartments. As TSG Positron Emission Particle Tracking (PEPT) studies have shown [36, 50], the material fill ratio before/in the kneading block is generally greater than that in the final conveying zone. This would extend the residence time of the kneading block and thereby reduce the time spent by particles in conveying sections. The fill level is known to play an important role in determining the shape and size of the particles since this determines the degree of compaction [31] and, again, may also protect particles from contacting the high shear boundary between the wall and the screw, thereby mitigating breakage [52]. This variation in mass distribution could be incorporated into the model by way of a flow model (such as that done for hot melt extrusion by Eitzlmayr et al. [21]) or, alternatively, by coupling the population balance to simulations using the Discrete Element Method (DEM), though such DEM couplings come at a high computational cost.

4.2 Evolution of the particle size distribution along the barrel

In this section the evolution of the model PSD is assessed along the length of the network (or equivalently, the length of the barrel) for an operating LSR of 0.25. Figure 6 shows the PSD in each compartment along the network and Table 3 details the optimised rate constants for each compartment.

We see that the dominant mechanism in the first compartment ($z = 1$) is nucleation, which causes a pronounced peak in the PSD around 2500μm. As a result of the bounds used for parameter estimation, in Table 3 we see that conveying-only compartments ($z = 1, 3$) are subject to a lower degree of breakage (k_{att}) relative to the compartment containing the kneading elements ($z = 2$). The reduced breakage rate allowed the oversized nucleates to co-exist with the remaining primary powder in a highly bimodal distribution, alluding to the inherent bimodality-by-liquid-inception suggested by Hagrasy et al. [26]. The position of the nuclei peak relative to the droplet size of 2000μm indicates that nuclei have been subjected to a moderate degree of compaction in the first compartment following their formation.

Moving from $z = 1$ to $z = 2$ in Figure 6, we see that a high degree of compaction and breakage has broken down the large nuclei into smaller, more dense fractions, consistent with the findings of Djuric and Kleinebudde [20]. We also note that the penetration rate constant has reached it's lower bound and this [process has effectively turned of. This is likely a reflection of the competition between the compaction and penetration processes in. These processes compete to move liquid to and from the surface of the particles, respectively. Thus the amount of surface liquid available during coagulation events is not sensitive to the absolute the value of k_{comp} and k_{pen} but rather their relative magnitudes. This coupling is undesired and is areas in which the model could be improved upon in the future. The squeezing effects of the compaction processes are further evident from the average particle composition statistics (Figure 7), in which a slight reduction in internal

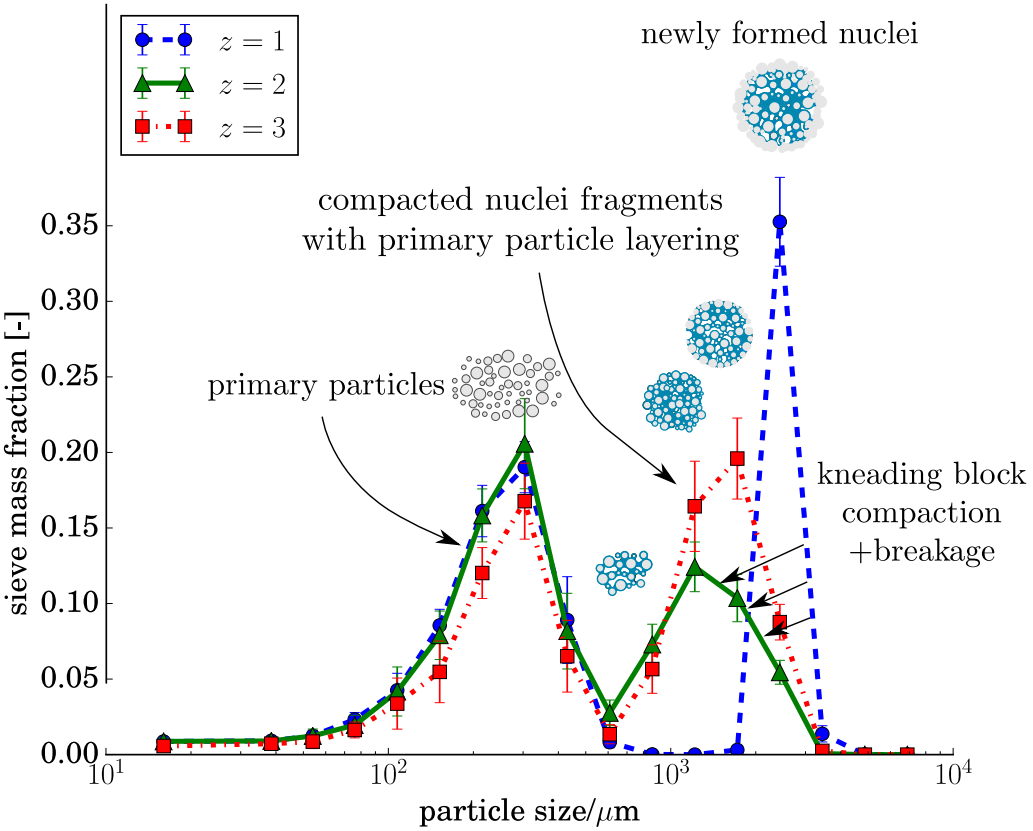

Figure 6: *Spatial PSD evolution for simulation with LSR=0.25.*

liquid (and resulting increase in external liquid) is evident in the transition between $z = 1$ and $z = 2$. This replicates the squeezing process within kneading blocks observed in numerous experimental studies [19, 22, 49, 55, 56].

It is also noted that breakage is the dominant process in the second compartment (kneading zone) and that the coagulation rate constant has reached it's lower bound, indicating very limited coagulation within this compartment. It is likely that similar ratios of k_{att} to k_{col} could feasibly generate similar size distributions within $z = 2$ due to the competing nature of the coagulation and breakage processes.

As the particles transition from the kneading zone to the final conveying zone, we observe a degree of coalescence between primary particles and compacted/surface wet agglomerates. At this stage the combination of moderate breakage and low compaction rate allows particles to grow whilst increasing in porosity (the reader is reminded that successful coalescence events result in an increase in particle pore volume in the model). This is in line with the production of large *friable* agglomerates from conveying only section observed in TSG and twin-screw extrusion systems [20].

Table 3: *Optimised rate constants.*

Compartment index z	1,3			2			1-3
Parameter	k_{col}	k_{att}	k_{comp}	k_{col}	k_{att}	k_{comp}	k_{pen}
Unit	m^3	m^{-1}s	-	m^3	m^{-1}s	-	$\text{kg}^{\frac{1}{2}}\text{m}^{-\frac{7}{2}}\text{s}^{-\frac{3}{2}}$
Value	1.21×10^{-10}	9.42×10^{6}	0.395	9.99×10^{-13}	1.09×10^{9}	0.954	10.0

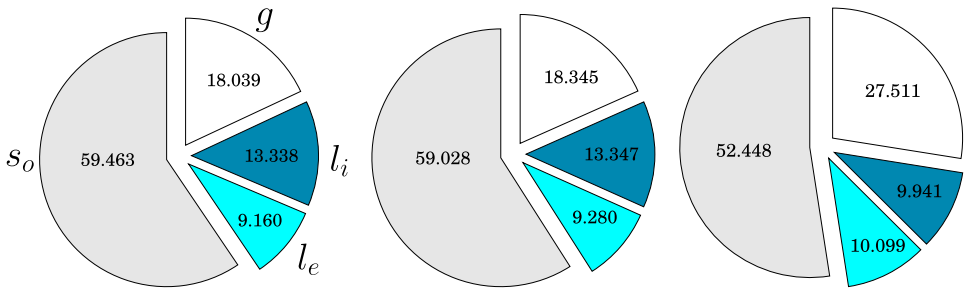

(a) $z = 1$ (b) $z = 2$ (c) $z = 3$

Figure 7: *Number averaged particle composition along the length of the compartment network with with an operating LSR=0.25.*

5 Conclusions and future recommendations

In this paper we have presented a high dimensional model for TSG which includes particles coagulation, compaction, breakage, penetration and nucleation. The model performed reasonably well against experiment at low LSR values but showed an over-prediction of fines at higher LSR values, resulting in a consistently bimodal PSD.

Based on the results of this study a number of recommendations for model improvements and future analysis can be made. Firstly, the introduction of a layering mechanism may mitigate the over-prediction of fines by the current model. This may also better reflect the difference between collision events involving a mixture of primary particles and agglomerates and those between agglomerates alone. Consideration of variable particle aspect ratios may be required to reflect the experimentally observed particle elongation. This is important both in the sieving process and in determining the likelihood of particle breakage/the resulting daughter distribution. It is also suggested that the population balance be coupled to a method for prediction of the mass distribution along the barrel from which compaction rates and residence times may be estimated. Finally, in order for optimised rates to be 're-used' across varying screw configurations the fitting methodology itself must be improved upon. In the future more advanced parameter optimisation could be carried out by fitting each compartmental PSD of the model against the experimental PSD at each associated barrel position, as carried out experimentally by Kumar et al. [31]. However, non-destructive extraction of a representative sample mid-barrel can be challenging. Alternatively, the model could be optimised against a large number of ex-

periments with varying screw configuration (such as that carried out by Vercruysse et al. [56]), in order to isolate the individual contributions of each group of elements. Another option is to perform optimisation of element specific rate constants based on experimental studies such as that by Sayin et al. [48]. Here the role of each element types is assessed by only supplying liquid at the very end of the barrel, such that only a short section of the twin-screw is active and the compounded effects of different elements in sequence are mitigated. However, it is likely that the role of specific screw elements is inherently coupled to the complete screw configuration and other processing conditions. It is more likely that a combination of these approaches will be required to build and refine future TSG models, gather element specific rate constants and move towards a truly modular TSG modelling framework.

Nevertheless, the stochastic method employed in the solution of this model, unlike traditional sectional methods, allows the dimensionality of the particle description to be readily extended to include many of the features that have been described above. These additional properties may then be incorporated into the particle transformations associated with TSG mechanisms. This makes this work an important step towards a quantitative prediction tool for formulation development with TSG systems.

In the second part of this study we present and analyse the properties of the numerical methodology employed to overcome the numerical challenges presented by twin-screw systems and solve the model presented in this paper.

Acknowledgements

The authors would like to thank AstraZeneca for funding this work. This project was partly funded by the National Research Foundation (NRF), Prime Minister's Office, Singapore under its Campus for Research Excellence and Technological Enterprise (CREATE) programme.

Nomenclature

Roman symbols

d	particle diameter	m
d_{max}	maximum primary particle diameter	m
d_{min}	minimum primary particle diameter	m
H_{a}	height of surface asperities	m
k_{att}	breakage rate constant	s m^{-1}
k_{col}	collision rate constant	m^3
k_{comp}	compaction rate constant	-
k_{pen}	penetration rate constant	$\text{kg}^{1/2}\text{m}^{-7/2}\text{s}^{-3/2}$
K_{col}	size independent collision kernel	s^{-1}
l_{e}	external liquid volume	m^3
l_{i}	internal liquid volume	m^3
$l_{\text{i}\rightarrow\text{e}}$	volume of liquid transferred to exterior during compaction	m^3
LSR	operating liquid solid mass flowrate ratio	-
$\bar{m}_{\text{feed}}$	number average feed particle mass	kg
$\dot{M}_{\text{feed}}$	solid mass flowrate	kg s^{-1}
n_{comp}	number of compartments	-
n_{screw}	screw speed	rev s^{-1}
N	number of particles	-
N_{exp}	number of experimental conditions	-
N_{response}	number of simulation/experimental responses	-
OF	fitting objective function	-
p	pore volume	m^3
P_{nuc}	probability of a particle being integrated into nucleus	-
Δp_{comp}	compaction pore reduction	m^3
q_0	primary particle number distribution	m^{-1}
q_3	primary particle volume distribution	m^{-1}
r_{break}	particle breakage rate	s^{-1}
r_{pen}	particle penetration rate	m^3s^{-1}
R_{incept}	primary particle inception rate	s^{-1}
$R_{\text{incept,droplet}}$	droplet inception rate	s^{-1}
R_{inflow}	particle inflow rate	s^{-1}
R_{nuc}	nucleation rate	s^{-1}
R_{outflow}	particle outflow rate	s^{-1}
s_{o}	original solid volume	m^3
s^*	pore saturation limit	-
t	time	s
T_{comp}	compaction transform	-
T_{break}	breakage operator	-

v	particle volume	m^3
v_{nuc}^{max}	maximum particle volume permitted to join nucleus	m^3
v_{parent}^{min}	minimum volume for breakage	m^3
v_{drop}	droplet volume	m^3
V_{real}	compartment volume	m^3
$V_{real,T}$	total volume of all compartments	m^3
V_{samp}	compartment sample volume	m^3
$\dot{V}_l$	binder flowrate	$m^3 s^{-1}$
w	particle statistical weight	-
x	particle vector	m^3
x_{nuc}	nuclei particle vector	m^3
x_{nuc}^{start}	initial nuclei particle vector	m^3
y_{exp}	experimental fitting response	m
y_{sim}	simulation fitting response	m
z	compartment index	-

Greek symbols

$\alpha_{daughter}$	breakage distribution parameter	-
$\beta_{daughter}$	breakage distribution parameter	-
ε	particle porosity	-
ε_{bed}	particle bed packing fraction	-
ε_{min}	minimum particle porosity	-
μ_{binder}	binder viscosity	Pa s
ρ_l	binder density	$kg\ m^{-3}$
ϕ	liquid saturation	-
ϕ_{max}	maximum liquid saturation	-
ϕ_{nuc}	nucleation liquid saturation	-
σ	fitting response scaling factor	m
τ	compartment residence time	s

References

[1] T. Allen. *Particle size measurement*. Springer, 2013.

[2] D. Barrasso and R. Ramachandran. Qualitative assessment of a multi-scale, compartmental PBM-DEM model of a continuous twin-screw wet granulation process. *Journal of Pharmaceutical Innovation*, 11(3):231–249, 2016. doi:10.1007/s12247-015-9240-7.

[3] D. Barrasso, T. Eppinger, F. E. Pereira, R. Aglave, K. Debus, S. K. Bermingham, and R. Ramachandran. A multi-scale, mechanistic model of a wet granulation process using a novel bi-directional PBM-DEM coupling algorithm. *Chemical Engineering Science*, 123:500 – 513, 2015. doi:10.1016/j.ces.2014.11.011.

[4] D. Barrasso, A. E. Hagrasy, J. D. Litster, and R. Ramachandran. Multi-dimensional population balance model development and validation for a twin screw granulation process. *Powder Technology*, 270, Part B:612 – 621, 2015. doi:10.1016/j.powtec.2014.06.035.

[5] D. Barrasso, A. Tamrakar, and R. Ramachandran. Model order reduction of a multi-scale pbm-dem description of a wet granulation process via ann. *Procedia Engineering*, 102(Supplement C):1295 – 1304, 2015. doi:doi.org/10.1016/j.proeng.2015.01.260.

[6] P. Bratley and B. L. Fox. Algorithm 659: Implementing Sobol's quasirandom sequence generator. *ACM Transactions on Mathematical Software*, 14(1):88–100, 1988. doi:10.1145/42288.214372.

[7] A. Braumann and M. Kraft. Incorporating experimental uncertainties into multivariate granulation modelling. *Chemical Engineering Science*, 65(3):1088 – 1100, 2010. doi:10.1016/j.ces.2009.09.063.

[8] A. Braumann, M. J. Goodson, M. Kraft, and P. R. Mort. Modelling and validation of granulation with heterogeneous binder dispersion and chemical reaction. *Chemical Engineering Science*, 62(17):4717 – 4728, 2007. doi:10.1016/j.ces.2007.05.028.

[9] A. Braumann, M. Kraft, and P. R. Mort. Parameter estimation in a multi-dimensional granulation model. *Powder Technology*, 197(3):196 – 210, 2010. doi:10.1016/j.powtec.2009.09.014.

[10] A. Braumann, M. Kraft, and W. Wagner. Numerical study of a stochastic particle algorithm solving a multidimensional population balance model for high shear granulation. *Journal of Computational Physics*, 229(20):7672 – 7691, 2010. doi:10.1016/j.jcp.2010.06.021.

[11] A. Braumann, P. L. W. Man, and M. Kraft. Statistical approximation of the inverse problem in multivariate population balance modeling. *Journal of Industrial and Engineering Chemistry*, 49(1):428–438, 2010. doi:10.1021/ie901230u.

[12] A. Braumann, P. L. W. Man, and M. Kraft. The inverse problem in granulation modeling-two different statistical approaches. *AIChE Journal*, 57(11):3105–3121, 2011. doi:10.1002/aic.12526.

[13] G. P. E. Brownbridge, A. Smallbone, W. Phadungsukanan, S. Mosbach, M. Kraft, and B. Johansson. Automated IC engine model development with uncertainty propagation. In *SAE Technical Paper*. SAE International, 04 2011. doi:10.4271/2011-01-0237.

[14] J. J. Cartwright, J. Robertson, D. D'Haene, M. D. Burke, and J. R. Hennenkamp. Twin screw wet granulation: Loss in weight feeding of a poorly flowing active pharmaceutical ingredient. *Powder Technology*, 238:116 – 121, 2013. doi:10.1016/j.powtec.2012.04.034.

[15] A. Chaudhury, M. E. Armenante, and R. Ramachandran. Compartment based population balance modeling of a high shear wet granulation process using data analytics. *Chemical Engineering Research and Design*, 95:211 – 228, 2015. doi:10.1016/j.cherd.2014.10.024.

[16] R. M. Dhenge, R. S. Fyles, J. J. Cartwright, D. G. Doughty, M. J. Hounslow, and A. D. Salman. Twin screw wet granulation: Granule properties. *Chemical Engineering Journal*, 164(2-3):322 – 329, 2010.

[17] R. M. Dhenge, J. J. Cartwright, D. G. Doughty, M. J. Hounslow, and A. D. Salman. Twin screw wet granulation: Effect of powder feed rate. *Advanced Powder Technology*, 22(2):162 – 166, 2011. doi:10.1016/j.apt.2010.09.004.

[18] R. M. Dhenge, J. J. Cartwright, M. J. Hounslow, and A. D. Salman. Twin screw granulation: Steps in granule growth. *International Journal of Pharmaceutics*, 438 (1-2):20 – 32, 2012.

[19] R. M. Dhenge, J. J. Cartwright, M. J. Hounslow, and A. D. Salman. Twin screw wet granulation: Effects of properties of granulation liquid. *Powder Technology*, 229: 126 – 136, 2012. doi:10.1016/j.powtec.2012.06.019.

[20] D. Djuric and P. Kleinebudde. Impact of screw elements on continuous granulation with a twin-screw extruder. *Journal of Pharmaceutical Sciences*, 97(11):4934–4942, 2008. doi:10.1002/jps.21339.

[21] A. Eitzlmayr, G. Koscher, G. Reynolds, Z. Huang, J. Booth, P. Shering, and J. Khinast. Mechanistic modeling of modular co-rotating twin-screw extruders. *International Journal of Pharmaceutics*, 474(1-2):157 – 176, 2014. doi:10.1016/j.ijpharm.2014.08.005.

[22] A. S. El Hagrasy and J. D. Litster. Granulation rate processes in the kneading elements of a twin screw granulator. *AIChE Journal*, 59(11):4100–4115, 2013. doi:10.1002/aic.14180.

[23] B. J. Ennis, G. Tardos, and R. Pfeffer. A special volume devoted to the second symposium on advances in particulate technology a microlevel-based characterization of granulation phenomena. *Powder Technology*, 65(1):257 – 272, 1991. doi:10.1016/0032-5910(91)80189-P.

[24] W. Ge, Y. Han, J. Wang, L. Wang, X. Liu, J. Zhou, J. Li, T. Freeman, A. Birkmire, and B. Armstrong. A QbD approach to continuous tablet manufacture. *Procedia Engineering*, 102:443 – 449, 2015. doi:10.1016/j.proeng.2015.01.185.

[25] M. Goodson, M. Kraft, S. Forrest, and J. Bridgwater. A multi-dimensional population balance model for agglomeration. In *PARTEC 2004:International Congress for Particle Technology*, 2004.

[26] A. E. Hagrasy, J. Hennenkamp, M. Burke, J. Cartwright, and J. Litster. Twin screw wet granulation: Influence of formulation parameters on granule properties and growth behavior. *Powder Technology*, 238:108 – 115, 2013. doi:10.1016/j.powtec.2012.04.035.

[27] R. Hooke and T. A. Jeeves. "Direct search" solution of numerical and statistical problems. *Journal of the ACM*, 8(2):212–229, Apr. 1961. doi:10.1145/321062.321069.

[28] M. J. Hounslow, R. L. Ryall, and V. R. Marshall. A discretized population balance for nucleation, growth, and aggregation. *AIChE Journal*, 34(11):1821–1832, 1988. doi:10.1002/aic.690341108.

[29] S. M. Iveson, J. D. Litster, K. Hapgood, and B. J. Ennis. Nucleation, growth and breakage phenomena in agitated wet granulation processes: a review. *Powder Technology*, 117(1-2):3 – 39, 2001. doi:10.1016/S0032-5910(01)00313-8.

[30] C. A. Kastner, G. P. Brownbridge, S. Mosbach, and M. Kraft. Impact of powder characteristics on a particle granulation model. *Chemical Engineering Science*, 97: 282 – 295, 2013. doi:10.1016/j.ces.2013.04.032.

[31] A. Kumar, J. Vercruysse, G. Bellandi, K. V. Gernaey, C. Vervaet, J. P. Remon, T. D. Beer, and I. Nopens. Experimental investigation of granule size and shape dynamics in twin-screw granulation. *International Journal of Pharmaceutics*, 475(1-2):485 – 495, 2014. doi:10.1016/j.ijpharm.2014.09.020.

[32] A. Kumar, J. Vercruysse, M. Toiviainen, P.-E. Panouillot, M. Juuti, V. Vanhoorne, C. Vervaet, J. P. Remon, K. V. Gernaey, T. D. Beer, and I. Nopens. Mixing and transport during pharmaceutical twin-screw wet granulation: Experimental analysis via chemical imaging. *European Journal of Pharmaceutics and Biopharmaceutics*, 87(2):279 – 289, 2014. doi:10.1016/j.ejpb.2014.04.004.

[33] A. Kumar, J. Vercruysse, V. Vanhoorne, M. Toiviainen, P.-E. Panouillot, M. Juuti, C. Vervaet, J. P. Remon, K. V. Gernaey, T. D. Beer, and I. Nopens. Conceptual framework for model-based analysis of residence time distribution in twin-screw granulation. *European Journal of Pharmaceutical Sciences*, 71:25 – 34, 2015.

[34] A. Kumar, J. Vercruysse, S. T. Mortier, C. Vervaet, J. P. Remon, K. V. Gernaey, T. D. Beer, and I. Nopens. Model-based analysis of a twin-screw wet granulation system for continuous solid dosage manufacturing. *Computers & Chemical Engineering*, 89:62 – 70, 2016. doi:10.1016/j.compchemeng.2016.03.007.

[35] K. F. Lee, S. Mosbach, M. Kraft, and W. Wagner. A multi-compartment population balance model for high shear granulation. *Computers & Chemical Engineering*, 75: 1 – 13, 2015. doi:10.1016/j.compchemeng.2015.01.009.

[36] K. T. Lee, A. Ingram, and N. A. Rowson. Twin screw wet granulation: The study of a continuous twin screw granulator using positron emission particle tracking (PEPT) technique. *European Journal of Pharmaceutics and Biopharmaceutics*, 81(3):666 – 673, 2012. doi:10.1016/j.ejpb.2012.04.011.

[37] H. Li, M. Thompson, and K. O'Donnell. Examining drug hydrophobicity in continuous wet granulation within a twin screw extruder. *International Journal of Pharmaceutics*, 496(1):3 – 11, 2015. doi:10.1016/j.ijpharm.2015.07.070.

[38] S. V. Lute, R. M. Dhenge, M. J. Hounslow, and A. D. Salman. Twin screw granulation: Understanding the mechanism of granule formation along the barrel length. *Chemical Engineering Research and Design*, 110:43 – 53, 2016. doi:10.1016/j.cherd.2016.03.008.

[39] P. L. Man, A. Braumann, and M. Kraft. Resolving conflicting parameter estimates in multivariate population balance models. *Chemical Engineering Science*, 65(13): 4038 – 4045, 2010.

[40] W. J. Menz, G. P. Brownbridge, and M. Kraft. Global sensitivity analysis of a model for silicon nanoparticle synthesis. *Journal of Aerosol Science*, 76:188 – 199, 2014. doi:10.1016/j.jaerosci.2014.06.011.

[41] MoDS. *(Model Development Suite)*. CMCL Innovations, Cambridge, United Kingdom, 2015. https://cmclinnovations.com/products/mods/.

[42] S. Mosbach, A. Braumann, P. L. Man, C. A. Kastner, G. P. Brownbridge, and M. Kraft. Iterative improvement of Bayesian parameter estimates for an engine model by means of experimental design. *Combustion and Flame*, 159(3):1303 – 1313, 2012.

[43] S. Mosbach, J. H. Hong, G. P. E. Brownbridge, M. Kraft, S. Gudiyella, and K. Brezinsky. Bayesian error propagation for a kinetic model of n-propylbenzene oxidation in a shock tube. *International Journal of Chemical Kinetics*, 46(7):389–404, 2014. doi:10.1002/kin.20855.

[44] M. Oullion, G. Reynolds, and M. Hounslow. Simulating the early stage of high-shear granulation using a two-dimensional Monte-Carlo approach. *Chemical Engineering Science*, 64(4):673 – 685, 2009. doi:10.1016/j.ces.2008.08.014.

[45] M. Pan, J. Sikorski, J. Akroyd, S. Mosbach, R. Lau, and M. Kraft. Design technologies for eco-industrial parks: From unit operations to processes, plants and industrial networks. *Applied Energy*, 175:305 – 323, 2016. doi:10.1016/j.apenergy.2016.05.019.

[46] D. Ramkrishna. *Population Balances: Theory and Applications to Particulate Systems in Engineering*. Elsevier Science, 2000.

[47] M. F. Saleh, R. M. Dhenge, J. J. Cartwright, M. J. Hounslow, and A. D. Salman. Twin screw wet granulation: Binder delivery. *International Journal of Pharmaceutics*, 487(1-2):124 – 134, 2015. doi:10.1016/j.ijpharm.2015.04.017.

[48] R. Sayin, A. E. Hagrasy, and J. Litster. Distributive mixing elements: Towards improved granule attributes from a twin screw granulation process. *Chemical Engineering Science*, 125:165 – 175, 2015. doi:10.1016/j.ces.2014.06.040.

[49] T. C. Seem, N. A. Rowson, A. Ingram, Z. Huang, S. Yu, M. de Matas, I. Gabbott, and G. K. Reynolds. Twin screw granulation - a literature review. *Powder Technology*, 276:89 – 102, 2015. doi:10.1016/j.powtec.2015.01.075.

[50] T. C. Seem, N. A. Rowson, I. Gabbott, M. de Matas, G. K. Reynolds, and A. Ingram. Asymmetric distribution in twin screw granulation. *European Journal of Pharmaceutics and Biopharmaceutics*, 106:50 – 58, 2016. doi:10.1016/j.ejpb.2016.01.013.

[51] U. Shah. Use of a modified twin-screw extruder to develop a high-strength tablet dosage form. *Pharmaceutical technology*, 29(6):52–66, 2005.

[52] M. Thompson and J. Sun. Wet granulation in a twin-screw extruder: Implications of screw design. *Journal of Pharmaceutical Sciences*, 99(4):2090–2103, 2010.

[53] W.-D. Tu, A. Ingram, and J. Seville. Regime map development for continuous twin screw granulation. *Chemical Engineering Science*, 87:315 – 326, 2013. doi:10.1016/j.ces.2012.08.015.

[54] V. Vanhoorne, B. Bekaert, E. Peeters, T. D. Beer, J.-P. Remon, and C. Vervaet. Improved tabletability after a polymorphic transition of delta-mannitol during twin screw granulation. *International Journal of Pharmaceutics*, 506(1-2):13 – 24, 2016. doi:10.1016/j.ijpharm.2016.04.025.

[55] J. Vercruysse, D. C. Díaz, E. Peeters, M. Fonteyne, U. Delaet, I. V. Assche, T. D. Beer, J. Remon, and C. Vervaet. Continuous twin screw granulation: Influence of process variables on granule and tablet quality. *European Journal of Pharmaceutics and Biopharmaceutics*, 82(1):205 – 211, 2012. doi:10.1016/j.ejpb.2012.05.010.

[56] J. Vercruysse, A. Burggraeve, M. Fonteyne, P. Cappuyns, U. Delaet, I. V. Assche, T. D. Beer, J. Remon, and C. Vervaet. Impact of screw configuration on the particle size distribution of granules produced by twin screw granulation. *International Journal of Pharmaceutics*, 479(1):171 – 180, 2015. doi:10.1016/j.ijpharm.2014.12.071.

[57] J. Vercruysse, E. Peeters, M. Fonteyne, P. Cappuyns, U. Delaet, I. V. Assche, T. D. Beer, J. Remon, and C. Vervaet. Use of a continuous twin screw granulation and drying system during formulation development and process optimization. *European Journal of Pharmaceutics and Biopharmaceutics*, 89:239 – 247, 2015. doi:10.1016/j.ejpb.2014.12.017.

[58] P. Vonk, C. Guillaume, J. Ramaker, H. Vromans, and N. Kossen. Growth mechanisms of high-shear pelletisation. *International Journal of Pharmaceutics*, 157(1): 93 – 102, 1997. doi:10.1016/S0378-5173(97)00232-9.